

Published in final edited form as:

*Lab Chip*. 2010 January 21; 10(2): 161–164. doi:10.1039/b917503b.

## Counting single molecules in sub-nanolitre droplets

T.D. Rane<sup>1,\*</sup>, C.M. Puleo<sup>1,\*</sup>, K.J. Liu<sup>1</sup>, Y. Zhang<sup>1</sup>, A.P. Lee<sup>2</sup>, and T.H. Wang<sup>1,3</sup>

T.D. Rane: tushar@jhu.edu; C.M. Puleo: cpuleo@jhu.edu; K.J. Liu: Kelvin@jhu.edu; Y. Zhang: yzhang68@jhmi.edu; A.P. Lee: aplee@uci.edu

<sup>1</sup> Johns Hopkins University, Department of Biomedical Engineering, 3400 N. Charles St., Clark Hall, Baltimore, MD, USA. Fax: 410-516-4771; Tel: 410-516-7576

<sup>2</sup> University of California, Irvine, Departments of Biomedical Engineering and Mechanical/Aerospace Engineering, ET 716F, Irvine, CA, USA Fax: 949-824-1727; Tel: 949-824-9691

### Abstract

We demonstrate single biomolecule detection and quantification within sub-nanolitre droplets through application of Cylindrical Illumination Confocal Spectroscopy (CICS) and droplet confinement within a retractable microfluidic constriction.

Droplet-based microfluidic platforms offer the distinct advantages of fast sample mixing, limited reagent dispersion, and lower sample loss or contamination when compared to traditional microfluidic devices.<sup>1, 2</sup> In addition, simple control strategies for kHz frequency droplet generation, transportation, storage, and sorting give the platform a propensity for high throughput analysis. While initial applications have been shown in a range of research disciplines, including biochemical analysis<sup>3</sup>, chemical and material synthesis<sup>4</sup>, and chemical reactions<sup>5</sup>, more recent applications have emerged that seek to expand this high throughput capability to the analysis of individual biological entities, such as single cells<sup>6–8</sup> or biomolecules.<sup>9, 10</sup>

In single cell experiments, *in vitro* compartmentalization in droplets enables rapid accumulation of secreted cellular factors<sup>11</sup>, and provides both chemical isolation and a unique means of cell selection and control.<sup>12</sup> Alternately, single molecule compartmentalization enables nucleic acid analysis through single-copy DNA PCR, extending the high throughput capacity of droplet-based microfluidics to digital PCR assays.<sup>7, 9, 10</sup> However, the current dependence on amplification techniques (e.g. PCR or fluorogenic substrate)<sup>1</sup> for detection of low concentration biomolecules presents limitations in droplet-based platforms; these include decreased throughput and added complexity involved with enzymatic amplification. These limitations point towards the need for integration of a highly sensitive detection platform for amplification-free detection of low-abundance biomolecules.

Confocal Fluorescence Spectroscopy (CFS) has traditionally been used for fluorescence based single molecule detection (SMD).<sup>13–18</sup> Resolution of single fluorophores is accomplished through reduction of a laser-illuminated probe volume to femtolitre size, thus minimizing background noise. Although well suited for SMD in continuous sample streams,

<sup>3</sup>Corresponding Author: Johns Hopkins University, Departments of Mechanical Engineering and Biomedical Engineering, 3400 N. Charles St., Latrobe Hall Rm. 108, Baltimore, MD, USA. Fax: 410-516-4316 ; Tel: 410-516-7086 ; thwang@jhu.edu.

\*TDR and CMP contributed equally to this work.

†Electronic Supplementary Information (ESI) available: S.1 – Device Fabrication and Operation, S.2 – Experimental Setup for SMD, S.3 – Sample Preparation, S.4 – Single Molecule Data Analysis

CFS is ill-suited for low abundance analyte detection in discrete volumes (e.g. droplets).<sup>19, 20</sup> Figure 1A depicts the challenges associated with SMD in droplet platforms. A single pass of the droplet through the laser illuminated volume results in low intra-droplet detection efficiencies (i.e. detection of only a small fraction of encapsulated molecules), as most biomolecules pass around the detection volume. In addition, even at nominal flow speeds the sub-nanolitre droplets pass by the detection volume in milliseconds, making it difficult to resolve 10's to 100's of molecules encapsulated within each single droplet.

In this report, we overcome challenges involved with biomolecular quantification in droplets, including short intradroplet signal acquisition times and droplet – illumination volume size mismatches. In our platform, one dimensional beam shaping using cylindrical optics (Cylindrical Illumination Confocal Spectroscopy, CICS)<sup>21</sup> produces a sheet-like illumination volume, maximizing intra-droplet detection efficiency (figure 1B). Furthermore, droplet confinement through a microfluidic constriction extends droplet duration through the illumination volume, providing the spatial and temporal resolution necessary to detect single biomolecules.

Controlled droplet confinement and passage through the illumination volume was accomplished using a microfluidic constriction channel patterned into a retractable PDMS valve (figure 1C). In the open valve state the constriction was not part of the fluidic path and presented no unnecessary challenge to droplet generation due to the increased fluidic resistance of the narrow channel. Water-in-oil droplets were generated using a flow-focusing configuration and transferred to a downstream storage chamber within the multilayered<sup>22</sup> PDMS device (details in S1, ESI). Upon valve actuation droplets were driven through the constriction using the continuous phase at a controlled pressure, while the occasional clogging of the narrow constriction was averted by pulsing the retractable channel to remove debris. The microdevices were coupled to a custom confocal fluorescence spectroscopic system as described previously<sup>19–21</sup>, by loading the chip onto a stage capable of sub-micron positioning of the chip relative to the illumination volume (details in S2, ESI). Two separate optical configurations were used with two different cylindrical lenses ( $f = 200$  mm or  $f = 300$  mm) to expand the illumination volume laterally across the constriction width, while remaining diffraction limited in the other dimensions to maximize signal to noise ratio (SNR).<sup>21</sup> These two configurations created detection volumes with  $14.3$  or  $64.6 \mu\text{m}^2$  cross-sections, respectively (details in S2, ESI). Four separate microdevices were fabricated with constrictions ranging from  $\sim 50 - 400 \mu\text{m}^2$  sized cross-sections, yielding a range of maximum possible molecular detection efficiencies (i.e ratio of the cross sectional areas of the laser illumination and the constriction channel) in traversing droplets from 3.5% to 100%.

Figure 2A shows that droplets from pL to nL sizes were stretched through the constrictions without droplet break-up. In the initial experiments, TOTO@-3 stained Lambda DNA was used as a model biomolecule. Varying concentrations of DNA were loaded in  $\sim 40$  pL droplets and run through the  $64.6 \mu\text{m}^2$  illumination volume held within the  $200 \mu\text{m}^2$  constriction. The raw data trace in figure 2B shows the outline of two control droplets (no DNA) running through the constriction (red trace – Fluorescence signal from Alexa 488 droplet indicator dye, black trace – Fluorescence signal from TOTO@-3/DNA; details in S3, ESI). Figure 2C shows the encapsulation and detection of the DNA at 37 pM concentrations. At these higher concentrations, droplet stretching through the constriction becomes increasingly essential as the  $\sim 1000$  DNA molecules per droplet (37 pM within 44.5 pL) must be resolved within the droplet's transit time through the CICS volume. Figure 3A shows the effect that droplet transit times had on single molecule counting at 37 pM. Burst counts per droplet approach a maximum value of 312 (red line – average of last three datapoints) at  $\sim 280$  ms. Droplets that traverse the constriction at a faster pace yield decreasing burst rates.

The lost information is a result of non-digital molecular occupancy in the illumination volume and decreased SNRs at faster speeds. However, the 312 average fluorescence bursts per droplet in the plateau region agree well with the expected value (320 bursts for the maximum possible detection efficiency of 32.3%). The small discrepancy from the expected value is attributable to molecular loss into the continuous phase and experimental variation in laser and constriction alignment (details of single molecule data analysis and thresholding in S4, ESI).

In all subsequent experiments, pressures that yielded equal droplet durations through the constriction were selected, yielding equal drop-to-drop acquisition times. This constraint enabled molecular quantification through the expected linear increase in single molecule fluorescent bursts with increasing molecular concentrations (figure 3B). In addition, the ability to mold intradroplet detection efficiencies via alterations in the constriction channel to laser illumination cross-section ratio is apparent in figure 3C. As shown, the average fluorescent bursts per droplet show a linearly increasing trend with decreasing constriction size at equivalent DNA concentrations (maximum possible detection efficiencies of 16.15, 32.3, 64.6, and 100 %; details in S1 and S2, ESI).

The results so far, indicate the effectiveness of the droplet-SMD platform in quantifying low abundance fluorescent biomolecules encapsulated within droplets. However, the utility of the droplet-SMD platform can also be extended to sequence specific nucleic acid assays using common single fluorophore nucleic acid probes.<sup>13, 15–18, 20</sup> As shown in figure 3D, a smaller CICS illumination volume ( $14.3 \mu\text{m}^2$ ) was used to increase SNR for single fluorophore studies. At 40 pM concentrations ( $\sim 1000$  molecules per 44.5 pL droplet), Cy5 molecular beacons (MB)<sup>20</sup> for E. coli rRNA sequences show few background peaks due to thermal fluctuation of the hairpin probe (Figure 3D top panel; average peaks per droplet  $0.282 \pm 0.11$ ). However, the presence of target is detectable upon target hybridization as an increase in fluorescence peak counts per drop (Figure 3D bottom panel; average peaks per droplet  $9.075 \pm 0.76$ ). These single fluorophore studies were performed using a  $200 \mu\text{m}^2$  constriction; however, the smaller constriction sizes used above demonstrate the ability to mold intradroplet detection efficiencies to meet a variety of experimental requirements.

In conclusion, for the first time we have demonstrated direct and amplification-free single molecule detection of biomolecules in sub-nanolitre droplets. As shown, biomolecular quantification using SMD requires only a microfluidic constriction channel for droplet confinement and elongation. Thus, the droplet-SMD microdevice presents a unique alternative to the complex PCR devices currently used for intra-droplet detection. Furthermore, by applying homogeneous probes for single molecule counting we were able to detect nucleic acids using a sequence specific probe. Future integration of the droplet-SMD platform with existing in-drop cell control and lysis techniques<sup>1, 2</sup> or single molecule probe schemes<sup>13, 15–18</sup> presents a general method for high-throughput single cell analysis.

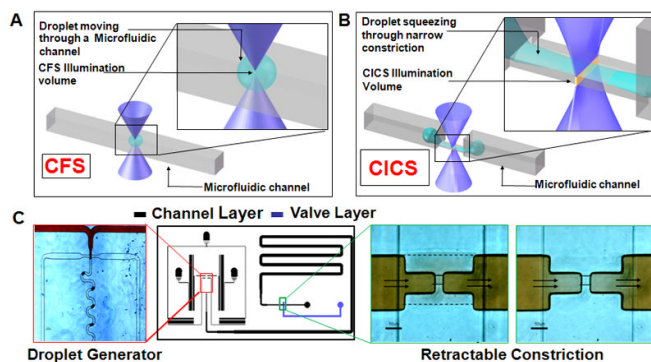
## Supplementary Material

Refer to Web version on PubMed Central for supplementary material.

## Notes and references

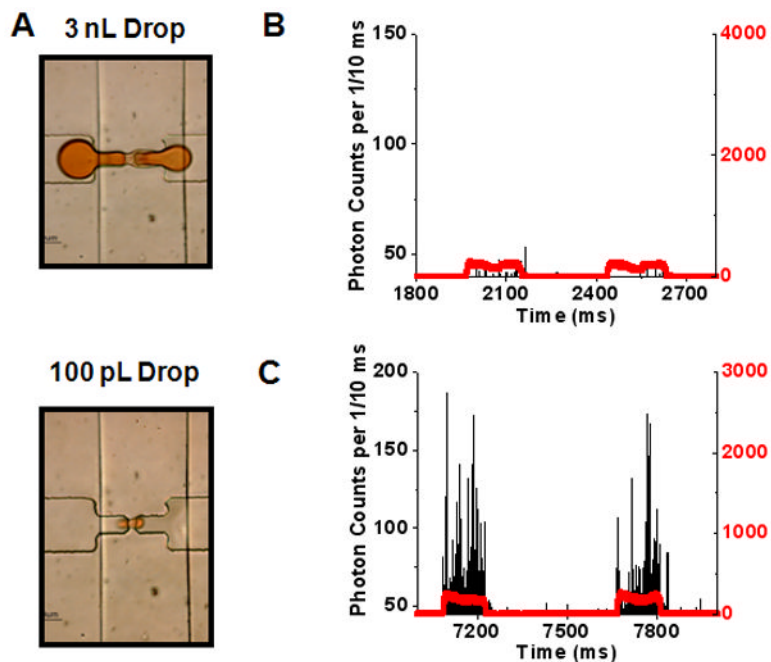
1. Teh SY, Lin R, Hung LH, Lee AP. Lab Chip 2008;8:198–220. 10.1039/b715524g. [PubMed: 18231657]
2. Huebner A, Sharma S, Srisa-Art M, Hollfelder F, Edel JB, Demello AJ. Lab Chip 2008;8:1244–1254. 10.1039/b806405a. [PubMed: 18651063]
3. Chiu DT, Lorenz RM. Acc Chem Res 2009;42:649–658. 10.1021/ar8002464. [PubMed: 19260732]

4. Nie Z, Xu S, Seo M, Lewis PC, Kumacheva E. *J Am Chem Soc* 2005;127:8058–8063. 10.1021/ja042494w. [PubMed: 15926830]
5. Song H, Chen DL, Ismagilov RF. *Angew Chem Int Ed Engl* 2006;45:7336–7356. 10.1002/anie.200601554. [PubMed: 17086584]
6. Huebner A, Srisa-Art M, Holt D, Abell C, Hollfelder F, deMello AJ, Edel JB. *Chem Commun (Camb)* 2007;(12):1218–1220. 10.1039/b618570c. [PubMed: 17356761]
7. Kumaresan P, Yang CJ, Cronier SA, Blazej RG, Mathies RA. *Anal Chem* 2008;80:3522–3529. 10.1021/ac800327d. [PubMed: 18410131]
8. Clausell-Tormos J, Lieber D, Baret JC, El-Harrak A, Miller OJ, Frenz L, Blouwolf J, Humphry KJ, Koster S, Duan H, Holtze C, Weitz DA, Griffiths AD, Merten CA. *Chem Biol* 2008;15:427–437. 10.1016/j.chembiol.2008.04.004. [PubMed: 18482695]
9. Schaeferli Y, Wootton RC, Robinson T, Stein V, Dunsby C, Neil MA, French PM, Demello AJ, Abell C, Hollfelder F. *Anal Chem* 2009;81:302–306. 10.1021/ac802038c. [PubMed: 19055421]
10. Beer NR, Wheeler EK, Lee-Houghton L, Watkins N, Nasarabadi S, Hebert N, Leung P, Arnold DW, Bailey CG, Colston BW. *Anal Chem* 2008;80:1854–1858. 10.1021/ac800048k. [PubMed: 18278951]
11. Boedicker JQ, Li L, Kline TR, Ismagilov RF. *Lab Chip* 2008;8:1265–1272. 10.1039/b804911d. [PubMed: 18651067]
12. Schmitz CH, Rowat AC, Koster S, Weitz DA. *Lab Chip* 2009;9:44–49. 10.1039/b809670h. [PubMed: 19209334]
13. Castro A, Williams JG. *Anal Chem* 1997;69:3915–3920. [PubMed: 9322430]
14. de Mello AJ. *Lab Chip* 2003;3:29N–34N. 10.1039/b304585b [doi].
15. Li H, Zhou D, Browne H, Balasubramanian S, Klenerman D. *Anal Chem* 2004;76:4446–4451. 10.1021/ac049512c [doi]. [PubMed: 15283586]
16. Neely LA, Patel S, Garver J, Gallo M, Hackett M, McLaughlin S, Nadel M, Harris J, Gullans S, Rooke J. *Nat Methods* 2006;3:41–46. nmeth825 [pii]; 10.1038/nmeth825 [doi]. [PubMed: 16369552]
17. Yeh HC, Chao SY, Ho YP, Wang TH. *Curr Pharm Biotechnol* 2005;6:453–461. [PubMed: 16375730]
18. Yeh HC, Ho YP, Shih I, Wang TH. *Nucleic Acids Res* 2006;34:e35. 34/5/e35 [pii]; 10.1093/nar/gkl021 [doi]. [PubMed: 16517937]
19. Puleo CM, Yeh HC, Liu KJ, Wang TH. *Lab Chip* 2008;8:822–822–825. 10.1039/b717941c. [PubMed: 18432356]
20. Puleo CM, Wang TH. *Lab Chip* 2009;9:1065–1072. 10.1039/b819605b. [PubMed: 19350088]
21. Liu KJ, Wang TH. *Biophys J* 2008;95:2964–2975. 10.1529/biophysj.108.132472. [PubMed: 18515376]
22. Unger MA, Chou HP, Thorsen T, Scherer A, Quake SR. *Science* 2000;288:113–116. 8400 [pii]. [PubMed: 10753110]



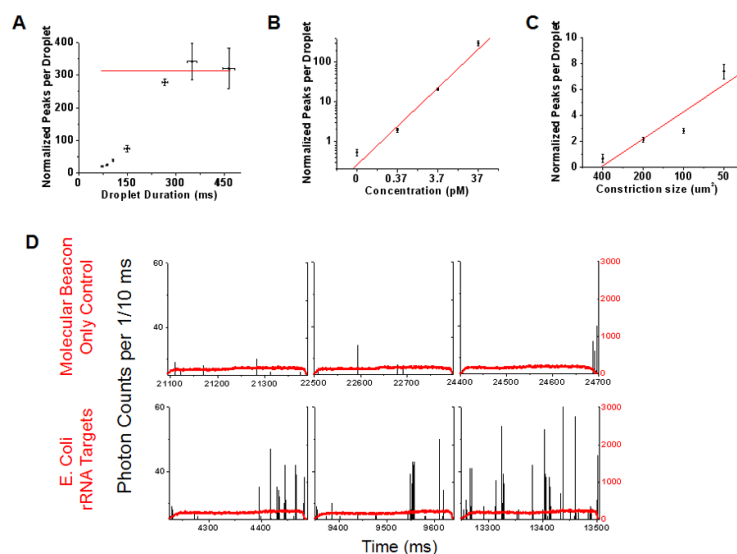
**Fig 1.**

**A.** A droplet moving through a microfluidic channel is shown. Inset shows the size of the droplet relative to the illumination volume of a standard Confocal Fluorescence Spectroscopy (CFS) setup. **B.** In contrast, elongation of a droplet squeezing through a microfluidic constriction is shown. The inset shows the sheet-like illumination volume of a Cylindrical Illumination Confocal Spectroscopy setup relative to the elongated droplet in the microfluidic constriction. **C.** The multilayered microfluidic device designed for the experiments in this paper is shown. A flow focusing geometry was used for droplet generation. The left panel shows droplets being generated using a food dye as the discrete phase. The rightmost panels show the retractable constriction region in either the open (left) or actuated (right) state, as described in text. (scale bar: 50  $\mu\text{m}$ )



**Fig 2.**

**A.** Retractable constriction in action: Two very different sized droplets can be seen stretching through the constriction without breakup. **B.** Sample single molecule trace data for control sample (TOTO@-3 dye only). The discrete phase consisted of 100 nM TOTO@-3 dye along with 100 nM Alexa 488 dye (Indicator dye). The red trace shows fluorescence signal from the indicator dye, while the black trace shows the fluorescence signal from TOTO@-3 dye. **C.** Similar single molecule trace data with the discrete phase consisting of TOTO@-3 labeled, 37 pM Lambda DNA and 100 nM Alexa 488 dye.

**Fig 3.**

**A.** Data showing the effect of droplet transit time on the mass detection efficiency within droplets. The data was obtained using a microfluidic chip (Fig 1C) with a  $200 \mu\text{m}^2$  constriction. The discrete phase consisted of  $1 \mu\text{M}$  TOTO-3,  $37 \text{ pM}$  Lambda DNA and  $100 \text{ nM}$  Alexa 488 dye. The number of single molecule fluorescent bursts increase with increasing droplet transit time through the microfluidic constriction, finally reaching a plateau (average value of  $312 \pm 31.9$ ; red line) at transit times  $>280 \text{ ms}$ . **B.** SMD-droplet platform response to changing molecular concentrations. Droplets were generated using discrete phase consisting of a range of DNA concentrations and passed through a  $200 \mu\text{m}^2$  constriction for single molecule detection. (Solid line: weighted linear regression,  $R = 0.989$ ) **C.** Manipulation of mass detection efficiency within droplets by simply changing the constriction size is demonstrated. As the constriction size decreases, larger sections of each droplet pass through the illumination volume and hence, mass detection efficiency increases. (Solid line: linear regression,  $R = 0.928$ ) All the experiments were conducted on a CICS setup with detection volume cross section size  $64.6 \mu\text{m}^2$  and DNA concentrations of  $0.37 \text{ pM}$  (details of data normalization in S4, ESI). **D.** The tunable nature of the droplet-CICS platform to attain single fluorophore sensitivity is illustrated using a Cy5 molecular beacon complementary to a sequence on 16S rRNA from E coli. The top row shows three representative sample droplets from a 'molecular beacon (MB) only' control sample. The black trace shows single molecule data from the Cy5 dye on the MBs. The bottom row shows sample droplets made from the same concentration molecular beacon hybridized with a synthetic target DNA. The average number of single molecule bursts per droplet in the control sample was  $0.282 \pm 0.11$ , compared to  $9.075 \pm 0.76$  in the target sample. This experiment was conducted on a chip with a constriction cross sectional area of  $200 \mu\text{m}^2$  and CICS illumination volume of  $14.3 \mu\text{m}^2$ . Each data point represents the interpolated y-intercept at zero threshold values from three sets of experiments with standard deviation; see details of single molecule analysis and thresholding in S4, ESI.